Microwave-Assisted Synthesis of Copper-Based Electrocatalysts for Converting Carbon Dioxide to Tunable Syngas

(Article begins on next page)

23 April 2024

CHEMELECTROCHEM

Supporting Information

Microwave-Assisted Synthesis of Copper-Based Electrocatalysts for Converting Carbon Dioxide to Tunable Syngas

Juqin Zeng,* Katarzyna Bejtka, Gaia Di Martino, Adriano Sacco, Micaela Castellino, Michele Re Fiorentin, Francesca Risplendi, M. Amin Farkhondehfal, Simelys Hernández, Giancarlo Cicero, Candido F. Pirri, and Angelica ChiodoniAn invited contribution to a Special Collection dedicated to Giornate dell'Elettrochimica Italiana 2019 (GEI2019)

Supporting information

Scheme of a microwave-assisted solvothermal route for preparing copper-based catalysts
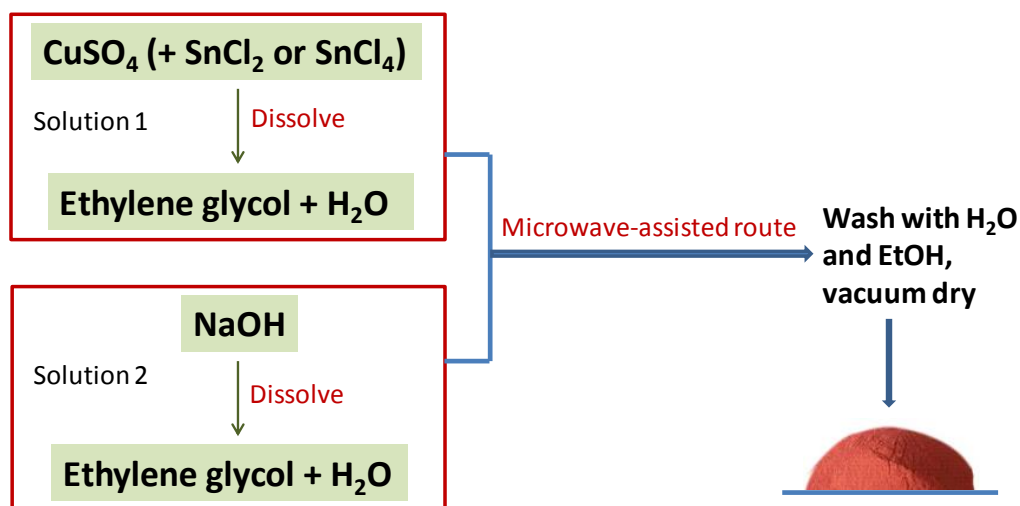
Scheme S1. A microwave-assisted solvothermal route for preparing copper-based catalysts.
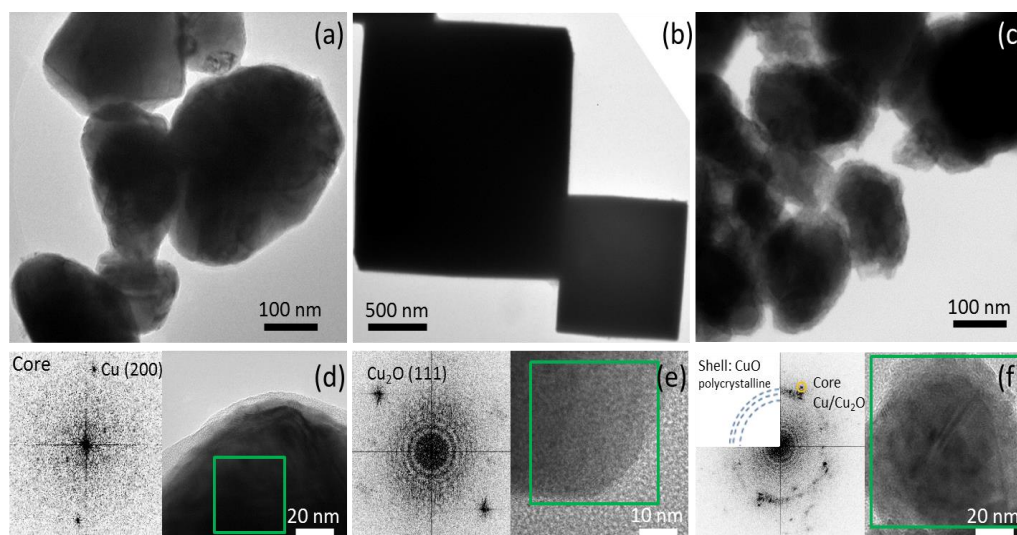
Detailed TEM analysis of the catalysts

Fig. S1 BF-TEM of Cu samples: (a and d) Cu-1; (b and e) Cu-5; (c and f) Cu-6. In the insets the FFT patterns obtained from the regions highlighted by frames.

Theoretical calculations

Our theoretical calculations are based on density functional theory (DFT) carried out with the Quantum Espresso suite [1]. Electronic wavefunctions are expanded in a plane-wave (PW) basis, exchange and correlation effects are modelled by the Perdew− Burke−Ernzerhof (PBE) functional [2] and the electron-ion interaction is described by optimized norm-conserving pseudopotentials [3]. For all calculations we adopted a PW energy cutoff of 80 Ry for the wavefunctions. All structures were relaxed by minimizing the atomic forces; convergence was assumed when the maximum component of the residual forces on the ions was smaller than 10^{-4} Ry/bohr. The Brillouin zone of the bulk Cu_2O unit cell was sampled using an 8×8×8 shifted Monkhorst-Pack mesh. The calculated lattice parameter of the Cu_2O cuprite structure is 4.311 Å, in good agreement with previous DFT results [4] and experimental values [5].

The thermodynamic study of surface stability focused on (110), (111), (200)-oxygen terminated and (200)-copper terminated surfaces. Each surface was modelled by employing 15-layer slabs with 15 Å of vacuum to ensure decoupling from periodic images along the z direction. The k-point grid was consistent with the one employed in the bulk system. The calculation of the surface energy followed the procedure detailed in Ref.[6], assuming thermodynamic equilibrium with oxygen gas. The surface energy curves at varying oxygen chemical potential are reported in Fig. S2. It is evident that the (200) surfaces are less stable than (111) and (110) in the whole variation range of the oxygen chemical potential. This shows that, in equilibrium and in the absence of other factors, cuprous oxide will not form cubic crystallites.
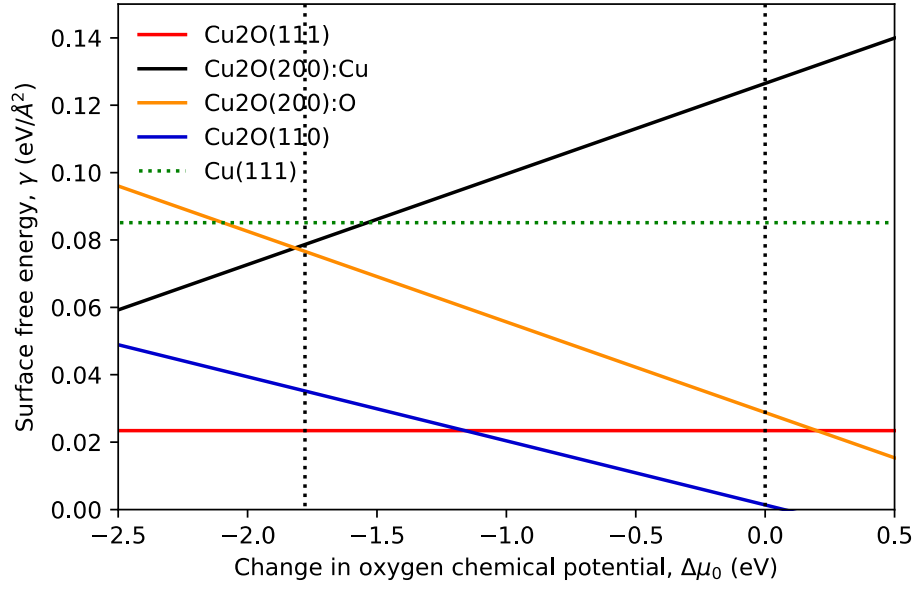
Fig. S2: Surface free energy variation of low-index Cu_2O surfaces with oxygen chemical potential.

EG adsorption was studied by focusing on the most stable Cu_2O surfaces, as from Fig. S2, namely (111), (110) and on (200)-oxygen terminated. For each considered surface, we employed a 2×2 surface supercell along the *a* and *b* lattice vectors, containing 7 layers. The lowest three layers were kept fixed in the bulk position. A 2×2×1 shifted k-point grid was used. A single EG molecule per supercell was adsorbed in a monodentate geometry for all surfaces, except for (200) in which case a bidentate geometry was also studied. The binding energy of adsorption was computed as

$$E_{ads} = E_{tot} - (E_{slab} + E_{EG}),$$

where E_{tot} and E_{slab} refer to the energy of the Cu_2O slab with the adsorbate and the Cu_2O slab alone, respectively, while E_{EG} is the energy of an EG molecule in a vacuum. Optimized adsorption geometries on the considered surfaces are displayed in Fig. S3.
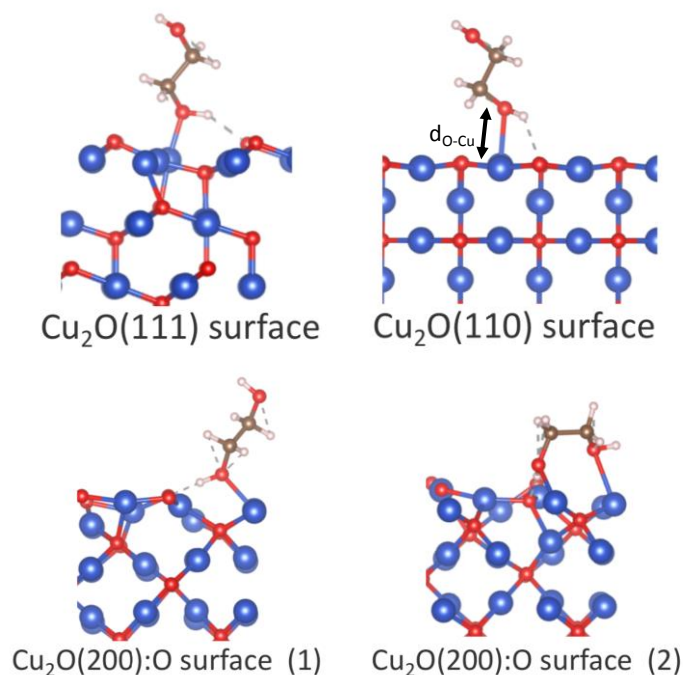
Fig. S3: Optimized adsorption geometries of EG on Cu$_2$O surfaces. On the (200):O both the monodentate and bidentate configurations are considered.

Bond distances and adsorption energies are reported in Table S1.

Table S1: Bond distances between EG bonding oxygen atom and surface copper atom (cf. Fig. S3) and binding energy for the EG adsorption on the considered surfaces. Cu$_2$O(200):O (1) refers to the monodentate geometry, while Cu$_2$O(200):O (2) to the bidentate setup.

	d_{O-Cu} (Å)	E_{ads} (eV)
Cu$_2$O (110)	4.467	-0.302
Cu$_2$O (111)	1.947	-1.496
Cu$_2$O (200):O (1)	2.070	-1.756
Cu$_2$O (200):O (2)	2.164 2.445	-2.108

In all cases, EG binds to a copper atom through one of its oxygen, highlighting the importance of the Cu-OH interaction. Deprotonation of EG was never observed in our simulations and was found to be energetically disfavored. The binding energy per Cu-O bond in the bidentate configuration, Cu$_2$O(200):O (2), is more positive than in the monodentate geometry. From Table S1 it is possible to conclude that EG is more strongly bound to the

(200) surface, both in the monodentate and bidentate configurations. This point at a net {100} surfaces stabilization and explains the ensuing crystallite cubic shape.

We used the double-layer capacitance (C_{dl}) value to evaluate the ESAs of the electrodes.

As shown in Fig. S4, the C_{dl} values of the various electrodes are evaluated by cyclic voltammetry (CV) at various scan rates in a potential range where no faradaic process occurs. The current intensities are plotted against the scan rates, and the slope of the linear fitting quantifies the double-layer capacitance C_{dl} of the electrodes (in Table S2).

Even though the complex nature of the Cu-based electrode (composition of CuO_x, carbon black CB and Nafion), we can reasonably calculate the ESA by comparing the C_{dl} of the electrode with a rather flat Cu foil. The CuO_x can be reduced to metallic Cu at potentials even more positive than +0.2 V vs. RHE. Hence, in the potential range where the C_{dl} is evaluated (from 0.0 to +0.2 V vs. RHE), 90 wt. % of the electrode is considered metallic Cu. We assume that the CuO_x-derived Cu metal is the main contributor to the C_{dl} of the electrode. Waszczuk et al. [7] reported a C_{dl} value of 28 µF cm^{-2} for a flat Cu electrode. The C_{dl} values of the Cu-based electrodes are divided by 28 µF cm^{-2}, resulting in the electrochemical surface area (ESA) of the electrodes, as shown in Table S2.

Table S2. Capacitance and ESA values of the electrodes.

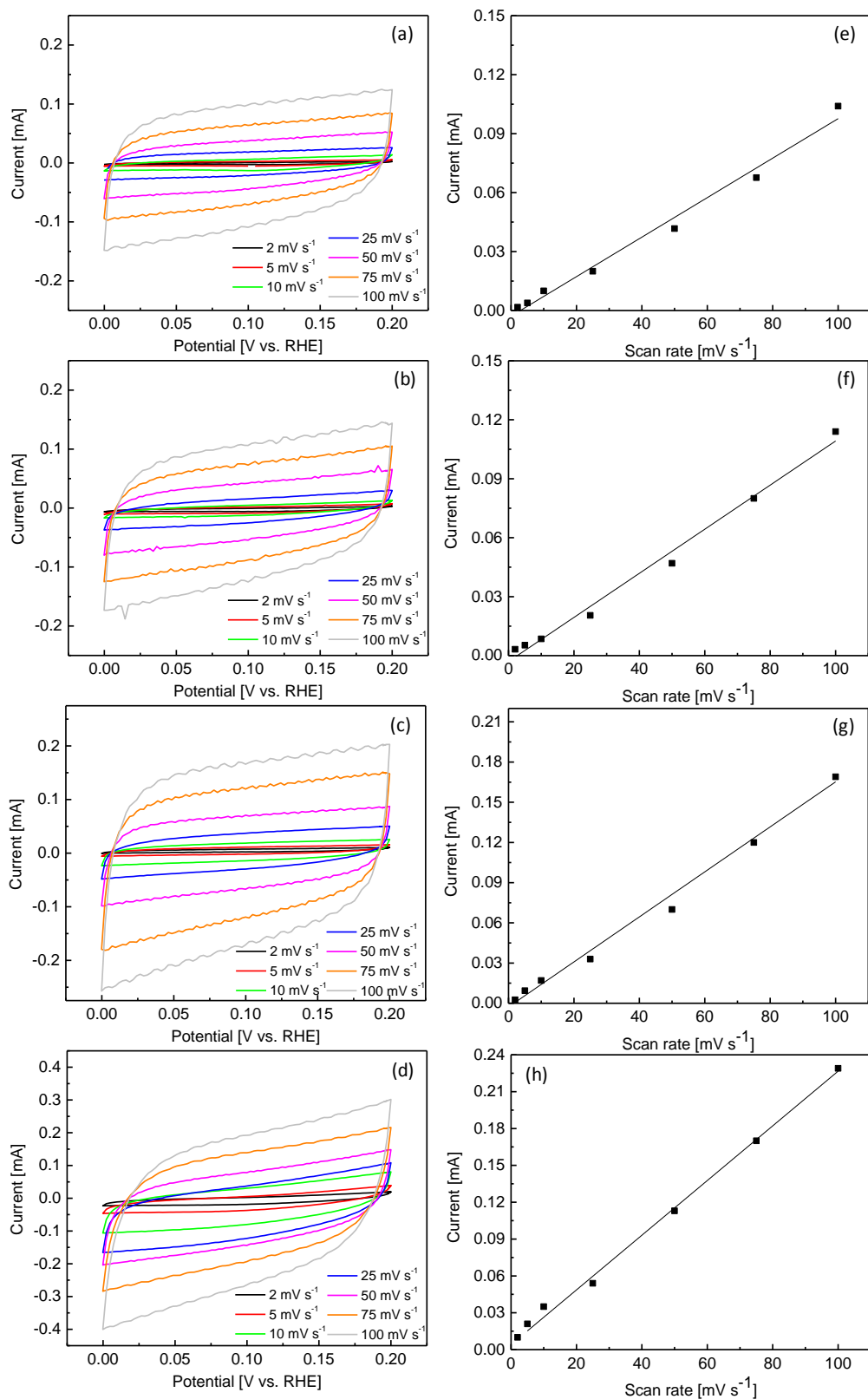| Electrode	C_{dl} (mF cm^{-2})	ESA (cm^2)
Cu foil	0.028	1
Cu-1	5.0	178
Cu-2	5.6	200
Cu-5	8.4	300
Cu-6	11.1	396

Fig. S4. Determination of C_{dl} for various electrodes (geometric area: 0.2 cm^2) in CO$_2$-saturated 0.1 M KHCO$_3$. CVs on electrodes (a) Cu-1; (b) Cu-3; (c) Cu-5; (d) Cu-6. Current intensities are plotted against the scan rates (e) Cu-1; (f) Cu-3; (g) Cu-5; (h) Cu-6.

Detailed chronoamperometric measurements at various potentials and analyses of products

on some catalysts
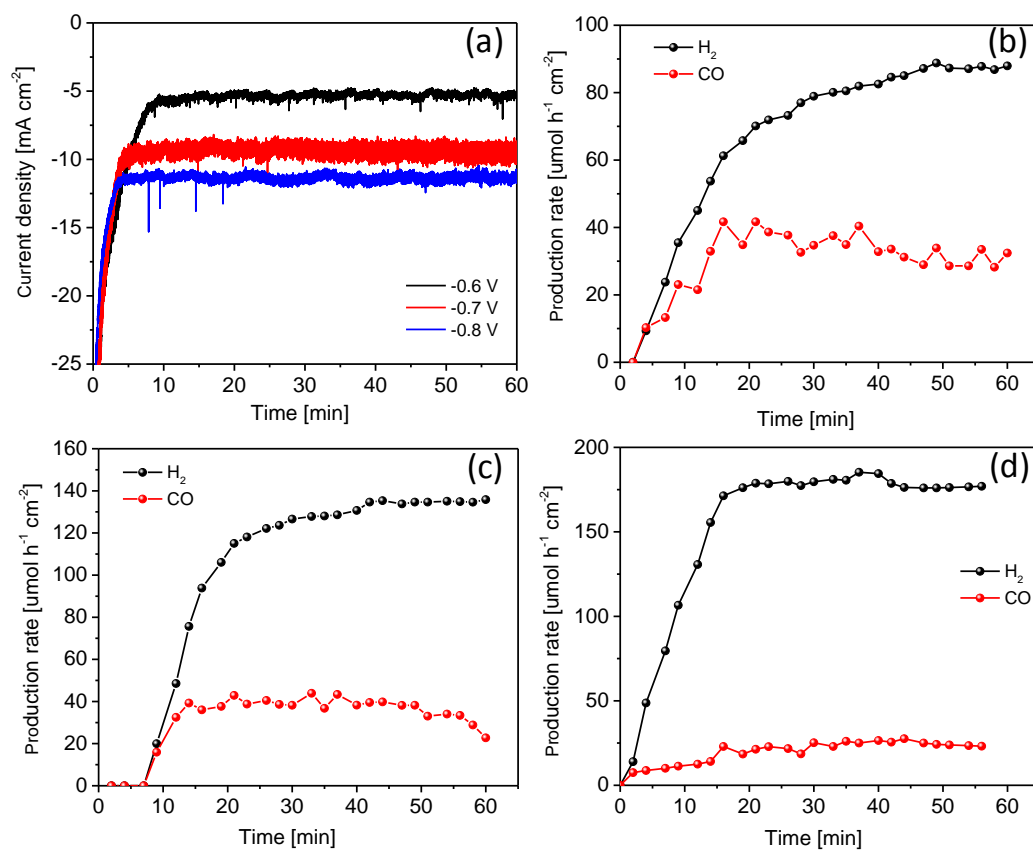

Fig. S5 CA measurements on the Cu-1 electrode in CO_2-saturated 0.1 M $KHCO_3$ aqueous solutions at various potentials (a). The production rates of H_2 and CO at various potentials: -0.6 V(b); -0.7 V (c); -0.8 V (d)

Fig. S6 CA measurements on the Cu-3 electrode in CO_2-saturated 0.1 M $KHCO_3$ aqueous solutions at various potentials (a). The production rates of H_2 and CO at various potentials: -0.6 V (b); -0.7 V (c); -0.8 V (d)
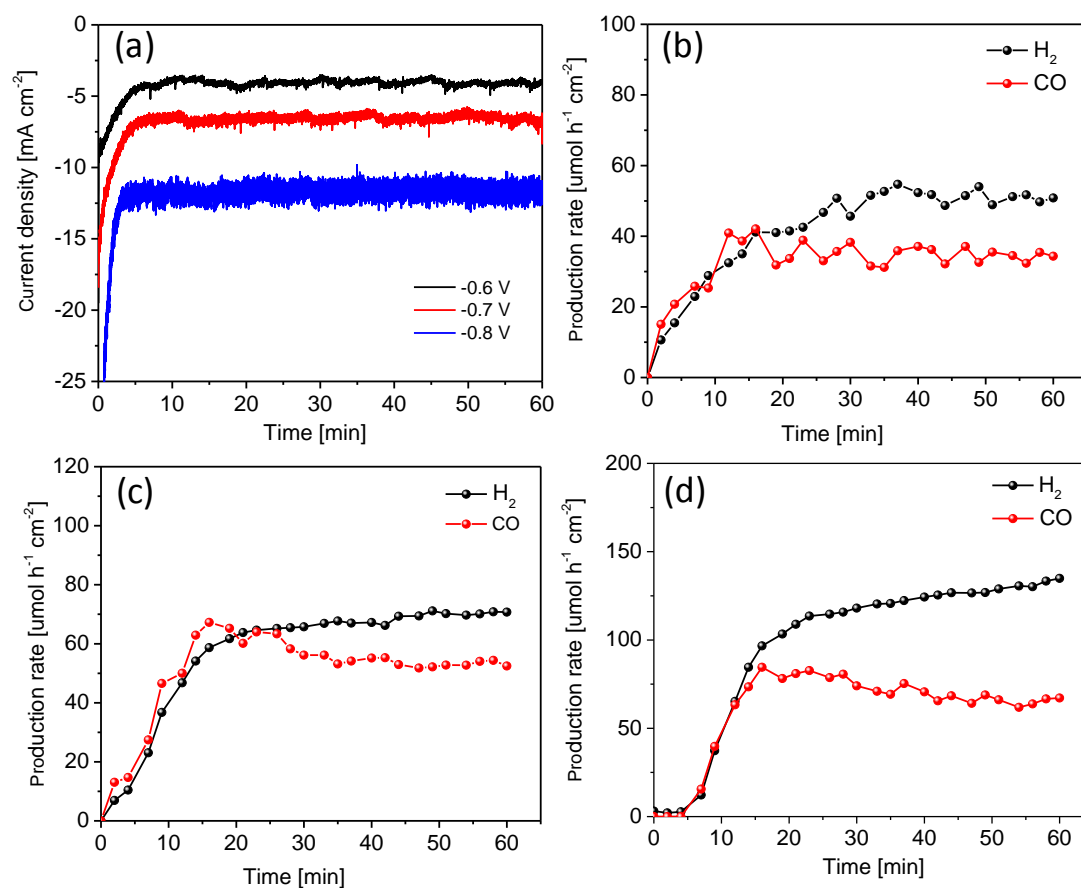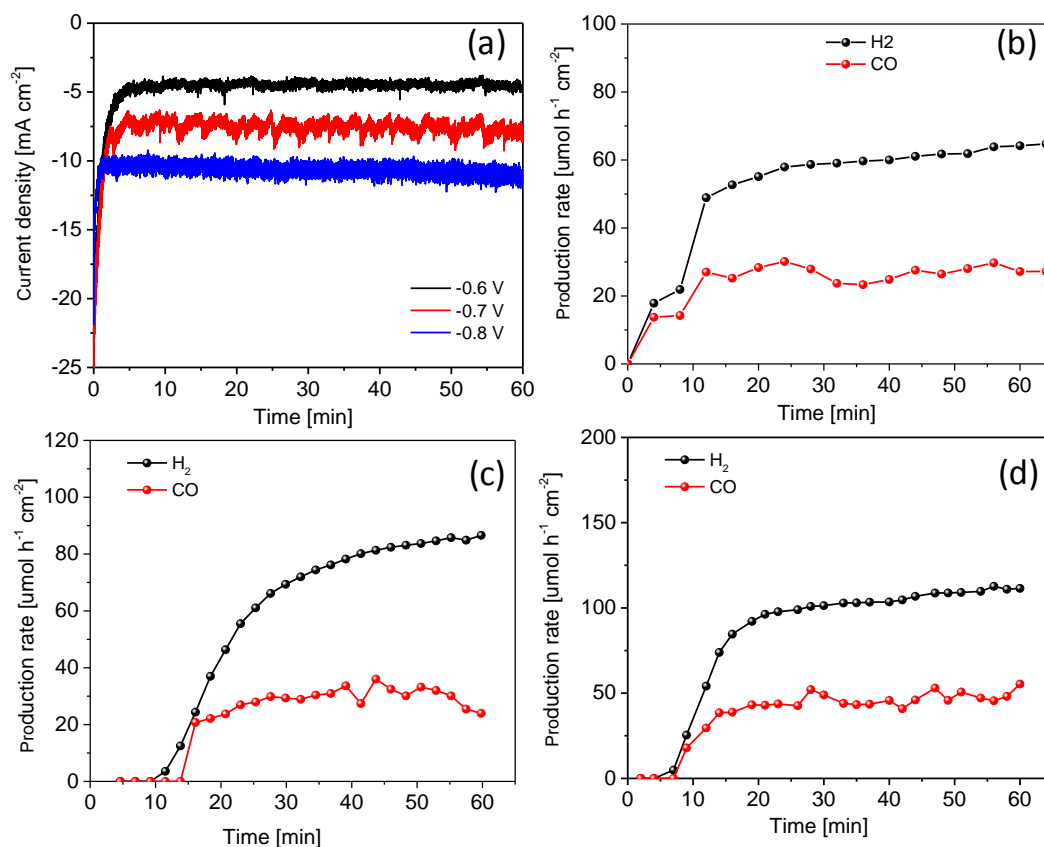
Fig. S7 CA measurements on the Cu-6 electrode in CO_2-saturated 0.1 M $KHCO_3$ aqueous solutions at various potentials (a). The production rates of H_2 and CO at various potentials: -0.6 V(b); -0.7 V (c); -0.8 V (d)

XRD characterization of the electrodes after test

As shown in Fig. S8, most of the material is reduced into metallic Cu after test, which is consistent with previous studies [8]. Some Cu_2O is also present, which may be due to the exposure to the air during the sample transfer. Different FWHM of the peaks implies different crystal sizes. In samples Cu-1, Cu-3 and Cu-6, the Cu peak is relatively narrow, suggesting that large crystals are formed. Meanwhile Cu-5 electrode shows broader Cu peak, and therefore smaller crystallites are expected.
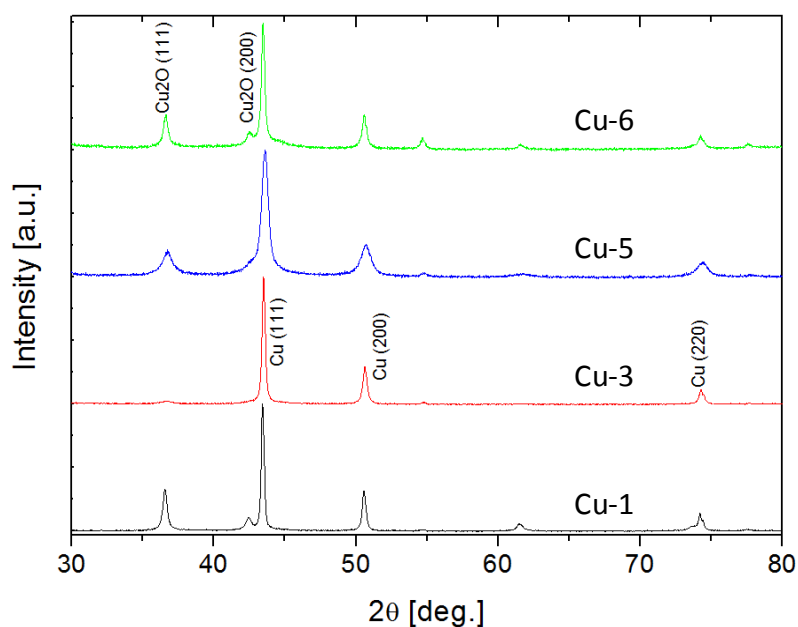

Fig. S8 XRD patterns of Cu-based electrodes after 1 hour of electrolysis.
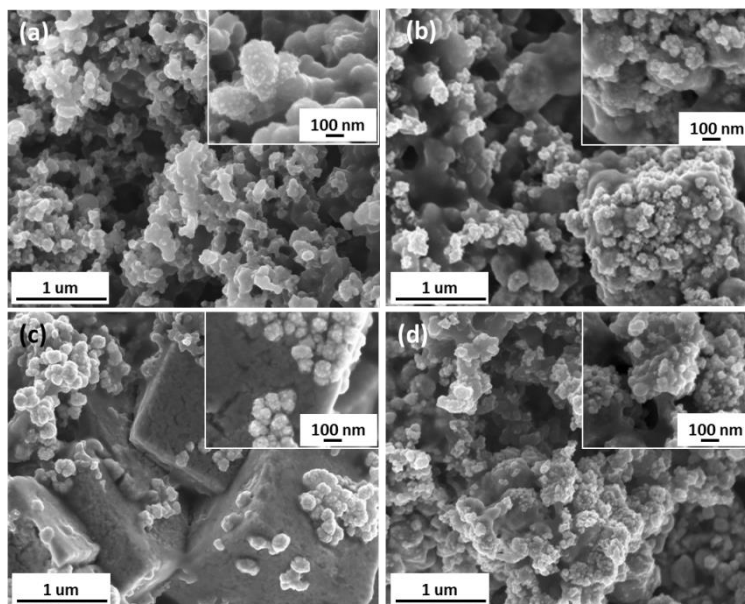
FESEM images of tested electrodes

Fig. S9 FESEM images of tested Cu electrodes: (a) Cu-1; (b) Cu-3; (c) Cu-5; (d) Cu-6.

Fig. S9 shows FESEM images of tested samples. It is important to note that these are images of electrodes, and therefore in addition to the active catalyst, carbon black and Nafion binder are also present. Besides the change of oxidation state of Cu (Fig. S8), the morphology is also changed. The surface of all the samples encounters potential-induced roughening during the CO_2RR. Especially, in Cu-5 electrode (Fig. S9c), cubic contours are still visible, but some evolution of the cube faces is evident. The cube walls are having rough appearance, suggesting being composed of small crystallites, with some small rounded particles present on it. This observation, in combination with the XRD results (Fig. S8), suggests the formation of a polycrystalline material with very small crystal size (even less than 10 nm) in the tested Cu-5 electrode. In addition, some of the material evolved into smaller round particles, which are now visible within the electrode.

References

[1] P. Giannozzi, S. Baroni, N. Bonini, M. Calandra, R. Car, C. Cavazzoni, D. Ceresoli, G. L. Chiarotti, M. Cococcioni, I. Dabo, A. Dal Corso, S. De Gironcoli, S. Fabris, G. Fratesi, R. Gebauer, U. Gerstmann, C. Gougoussis, A. Kokalj, M. Lazzeri, L. Martin-Samos, N. Marzari, F. Mauri, R. Mazzarello, S. Paolini, A. Pasquarello, L. Paulatto, C. Sbraccia, S. Scandolo, G. Sclauzero, A. Seitsonen, P., A. Smogunov, P. Umari, R. M. Wentzcovitch., *J. Phys.: Condens. Matter* **2009**, *21*, 395502.

[2] J.P. Perdew, K. Burke, M. Ernzerhof, *Phys. Rev. B* **1996**, *54*, 16533-16539.

[3] D.R. Hamann, *Phys. Rev. B* **2013**, *88*, 085117.

[4] A. Soon, M. Todorova, B. Delley, C. Stampfl*, Phys. Rev. B* **2006**, *73*, 165424.

[5] W.G. Wickoff, *Crystal structures* **1960**, Wiley-Interscience, New York.

[6] A. Soon, M. Todorova, B. Delley, C. Stampfl, *Phys. Rev. B* **2007**, *75*, 125420.

[7] P. Waszczuk, P. Zelenay, J. Sobkowski, Electrochim. Acta **1995**, *40*, 1717-1721.

[8] J. Zeng, K. Bejtka, W. Ju, M. Castellino, A. Chiodoni, A. Sacco, M. A. Farkhondehfal, S. Hernández, D. Rentsch, C. Battaglia, C. F. Pirri, *Appl. Catal., B* **2018**, *236*, 475-482.